

Article

Response Spectra-Based Post-Earthquake Rapid Structural Damage Estimation Approach Aided with Remote Sensing Data: 2020 Samos Earthquake

Onur Kaplan *  and Gordana Kaplan 

Institute of Earth and Space Sciences, Eskisehir Technical University, 26555 Eskisehir, Turkey; kaplangorde@gmail.com

* Correspondence: onur_kaplan@eskisehir.edu.tr; Tel.: +90-532-694-7905

Abstract: Effective post-event emergency management contributes substantially to communities' earthquake resilience, and one of the most crucial actions following an earthquake is building damage assessment. On-site inspections are dangerous, expensive, and time-consuming. Remote sensing techniques have shown great potential in localizing the most damaged regions and thus guiding aid and rescue operations in recent earthquakes. Furthermore, to prevent post-earthquake casualties, heavily damaged, unsafe buildings must be identified immediately since in most earthquakes, strong aftershocks can cause such buildings to collapse. The potential of the response spectrum concept for being associated with satellite-based remote sensing data for post-earthquake structural damage estimation was investigated in this study. In this respect, a response spectra-based post-earthquake structural damage estimation method aided by satellite-based remote sensing data was proposed to classify the buildings after an earthquake by prioritizing them based on their expected damage levels, in order to speed up the damage assessment process of critical buildings that can cause casualties in a possible strong aftershock. A case study application was implemented in the Bayrakli region in Izmir, Turkey, the most affected area by the Samos earthquake, on 30 October 2020. The damage estimations made in this research were compared with the in situ damage assessment reports prepared by the Republic of Turkey Ministry of Environment and Urbanization experts. According to the accuracy assessment results, the sensitivity of the method is high (91%), and the necessary time spent by the in situ damage assessment teams to detect the critical buildings would have been significantly reduced for the study area.



Citation: Kaplan, O.; Kaplan, G. Response Spectra-Based Post-Earthquake Rapid Structural Damage Estimation Approach Aided with Remote Sensing Data: 2020 Samos Earthquake. *Buildings* **2022**, *12*, 14. <https://doi.org/10.3390/buildings12010014>

Academic Editors: Tom Lahmer, Ehsan Harirchian and Viviana Novelli

Received: 28 November 2021

Accepted: 23 December 2021

Published: 26 December 2021

Publisher's Note: MDPI stays neutral with regard to jurisdictional claims in published maps and institutional affiliations.



Copyright: © 2021 by the authors. Licensee MDPI, Basel, Switzerland. This article is an open access article distributed under the terms and conditions of the Creative Commons Attribution (CC BY) license (<https://creativecommons.org/licenses/by/4.0/>).

Keywords: response spectrum; rapid damage assessment; remote sensing; deep learning

1. Introduction

A magnitude M_w 7.0 earthquake struck offshores of Samos Island (Greece) in the eastern Aegean Sea on 30 October 2020. Two people lost their lives, and many buildings were damaged or collapsed due to the earthquake in Karlovasi–Samos Island, Greece. However, the main effect of the earthquake was on the city of Izmir, Turkey, located about 65 km from the earthquake epicenter. Twelve buildings suffered an immediate collapse, and many buildings experienced heavy damage. One hundred and seventeen lives were lost, according to Turkey's Ministry of Interior Disaster and Emergency Management Presidency (AFAD) reports. The majority of the damages were located in the Bayrakli region because of amplified ground motion, despite the long distance from the source [1]. The presence of soft stories, lack of proper detailing, poor construction quality, the presence of heavy overhangs, and lack of code compliance were attributed as the primary causes of damage. The earthquake also demonstrated the effect of infill walls on the seismic performance of deficient and inadequate buildings [2].

Rapid urbanization poses a significant challenge to earthquake resilience in cities. The effective management of the post-event emergency contributes significantly to resilience,

and one of the most critical activities following an earthquake is assessing building damage [3]. Earthquake-induced building damage and collapse is a major cause of human casualties. In situ expert inspections are risky, expensive, and time-consuming. Therefore, rapid and reliable identification of areas affected by an earthquake is vital in activating appropriate aid and rescue missions after the disaster. In addition, to prevent post-earthquake casualties, the risky, heavily damaged buildings must be detected immediately because, in most earthquakes, strong aftershocks can cause the collapse of those buildings. In recent earthquakes, the use of satellite imagery has demonstrated great promise in localizing the most damaged areas and thus guiding rescue and reconstruction operations. Recent studies have reported that high-resolution satellite imagery can be used to detect post-seismic building damage [4–7].

Inspired by the success of deep learning methods for semantic segmentation in computer vision fields, many researchers have been focusing on Convolutional Neural Networks (CNN) for object detection from remote sensing data. CNN, a deep learning supervised neural network which uses labeled data, has been recognized as one of the most successful and widely used deep learning approaches [8,9]. For example, CNN has been used for object detection of trees [10–15], buildings extraction [16,17], ship detection [18,19], etc.

The potential of the response spectrum concept for being associated with satellite-based remote sensing data for post-earthquake structural damage estimation was investigated in this study. The response spectrum concept was first introduced in the mid-1930s. By the late-1960s, the elastic response spectrum was well developed and understood. This concept is very well integrated with both earthquake engineering practice and research [20]. The elastic response spectrum is plotted between the maximum response of single-degree-of-freedom (SDOF) systems subjected to a particular component of a ground motion and natural periods of SDOF systems. Each response spectrum has a fixed damping ratio ξ ; the damping ratio is usually expressed as a proportion of the critical damping, which returns a displaced oscillator to rest without any vibrations, called equivalent viscous damping [21]. In earthquake engineering, 5% of critical damping is generally used for reinforced concrete buildings. Response spectra can be plotted for the natural period T_n vs. acceleration, velocity, or displacement. For example, an acceleration response spectrum of a ground motion component gives the maximum acceleration response of an SDOF system for a given period. In other words, investigating the spectrum, it can be said that for which natural periods the SDOF system will be exposed to more immense accelerations or vice versa. It should be noted that most of the buildings in practice are multi-degree-of-freedom (MDOF) systems, and different modes contribute to their behavior. However, it can be assumed that the fundamental vibration mode controls the seismic response, at least for the buildings whose response is not affected by the contribution of higher modes of vibration (mid-rise buildings) and the buildings without torsional irregularities.

Regarding this, the fundamental vibration period of a building is a crucial parameter for earthquake engineering in both earthquake-resistant design and seismic performance assessment. The equivalent seismic lateral force is determined from a design spectrum in most static design methods. Consequently, the earthquake force is a function of the fundamental vibration period of the building [22,23]. The fundamental period can be computed based on modeling or simplified empirical relationships defined in seismic design codes. For rapid assessment applications, empirical equations are preferable. Kaplan et al. (2021) [24] developed an empirical relationship to predict elastic fundamental vibration periods of reinforced concrete buildings with masonry infill walls. The equation estimates the elastic fundamental period (T_0 , in seconds) with respect to building height (H , in meters) (Equation (1)). This equation was established by performing ambient vibration measurements on residential mid-rise reinforced concrete buildings in Eskisehir, Turkey. As being such, it may represent the typical dynamic characteristics of Turkish RC building stock.

$$T_0 = 0.0195H \quad (1)$$

The fundamental period can also be used to estimate the seismic demand during and after an earthquake using the response spectrum of the ground motion. This research aims to propose a response spectra-based post-earthquake structural damage estimation method aided by satellite-based remote sensing data. The research question that motivates this study is, “Can we classify buildings after an earthquake by prioritizing them based on their expected damage levels using the response spectra and remote sensing data?”, in order to speed up the damage assessment process of critical buildings that can cause casualties in a possible strong aftershock. For this purpose, a case study application was implemented in the Bayrakli region in Izmir, Turkey, the most affected area by the Samos earthquake on 30 October 2020. A CNN model was applied to extract buildings from high-resolution satellite imagery to detect the buildings in the study area affected by the earthquake. In addition, satellite images were used to determine the height of the buildings. Furthermore, Equation (1) was used to predict the fundamental vibration periods of the buildings based on the calculated heights. The obtained data were imported into a geographic information system (GIS) environment and further used for seismic damage estimation of the detected buildings. The seismic demand for the buildings was estimated by comparing fundamental vibration periods of the buildings with the response spectra of the ground motion recorded at the critical station near the most affected area. The produced information was used to prioritize the in situ damage assessment interventions in the affected region.

The main contributions of the study are as follows:

- (i) Using a CNN to extract buildings from high-resolution remote sensing imagery pre- and post-earthquake and thus, detect collapsed buildings;
- (ii) Using shadow information from high-resolution satellite imagery to calculate building heights;
- (iii) Estimation of fundamental vibration periods of detected buildings using the calculated building heights;
- (iv) Comparing the fundamental periods with the response spectra of ground shaking gathered from the critical accelerometer station for predicting damaged buildings;
- (v) Proposing a model for rapid damage estimation and prediction for post-earthquake analyses.

The paper has been organized into five sections. Information about the methods and materials on both remote sensing and the response spectra-based damage estimation and the study area details are given in Section 2. The results are presented in Section 3, while Sections 4 and 5 present the discussion and conclusion.

2. Materials and Methods

2.1. Study Area

The earthquake on 30 October 2020, on Samos Island caused significant damage to the city of Izmir. Izmir is the third-largest city of Turkey with a provincial population of 4.5 million, located approximately 65 km from the earthquake epicenter [25]. The city of Izmir is located on the Inner Bay of Izmir. Inner Izmir Bay is a shallow marine basin that is actively growing and is controlled by active east–west trending extensional faults (normal faults) in the Aegean Extensional Province. The uppermost sediments in the basin are young alluvium and fan-delta to shallow marine deposits confined and controlled by the Izmir Fault to the south and the Karsiyaka–Bornova fault to the north [26]. Soft alluvial soils amplified the spectral accelerations, especially in the Bayrakli region, and consequently, most of the heavy damage in buildings occurred in Bayrakli. The study area was chosen from this region, where five buildings collapsed, and seven buildings were heavily damaged (demolished after the earthquake) (Figure 1). The majority of the heavily damaged buildings were constructed in the 1990s with poor code compliance and construction quality. Moreover, some of the buildings’ structural systems were suspected to be modified to accommodate commercial use on the first floors [26]. Some of the substandard buildings in the region experienced gravity (pancake) type, and some of them sideways collapse [27] (Figure 2).

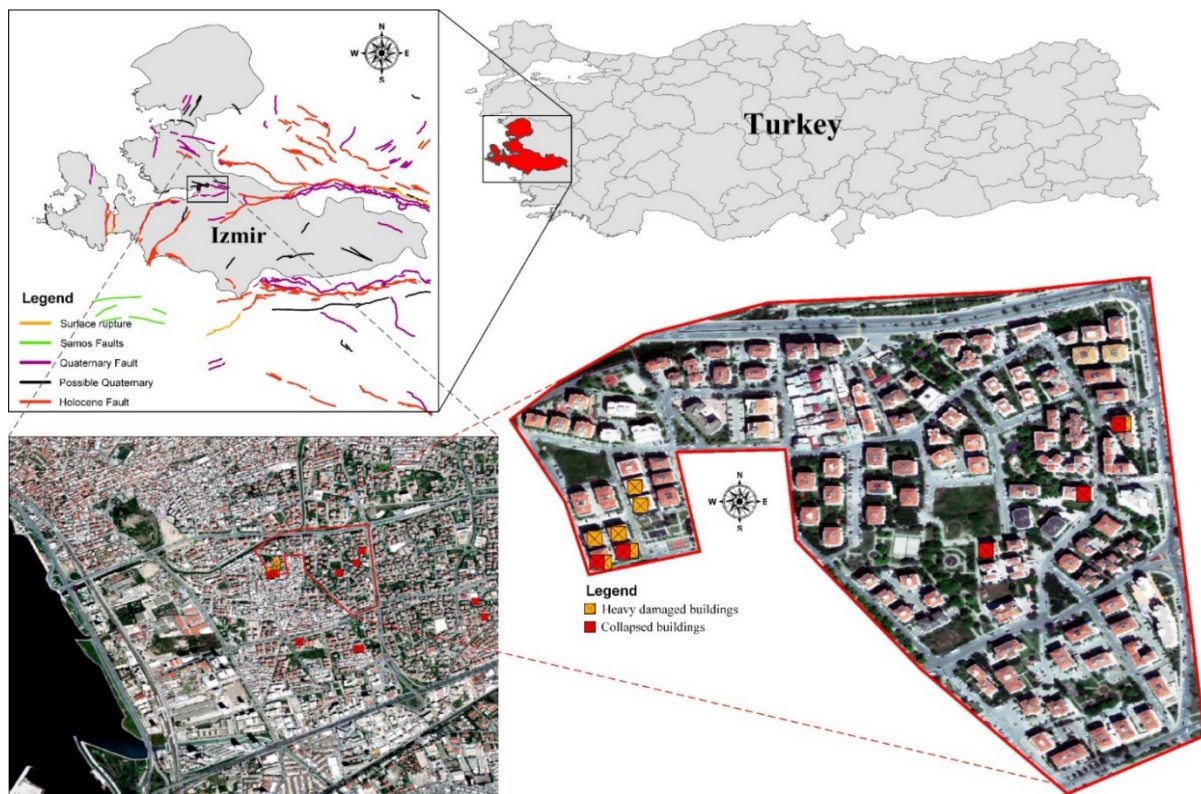


Figure 1. Study area.



Figure 2. Images from collapsed buildings in the Bayrakli region of Izmir [28,29].

2.2. Methodology

The presented study was carried out in two parts; remote sensing and structural damage estimation; then, the results of the two parts were compiled and assessed. The remote sensing part consists of four steps: (i) preparing the satellite data; (ii) implementing the CNN model for building extraction; (iii) assessment of the classification results; (iv) estimating the building heights using shadow lengths of the buildings. The structural damage estimation part also consists of six steps: (i) gathering real-time acceleration data from the stations located in the most affected area; (ii) deciding the critical station

and computing response spectra of its both horizontal components; (iii) determining the critical period intervals of the selected critical station's response spectra; (iv) estimating fundamental vibration periods of the surrounding buildings according to the building heights retrieved from remote sensing data; (v) comparing the fundamental periods with the response spectra of ground motion gathered from the critical station for estimating damaged buildings; (vi) the accuracy assessment of the proposed approach has been conducted comparing the estimation results with the in situ damage assessment reports. The details about the methodology implemented in the study are presented in the flowchart shown in Figure 3.

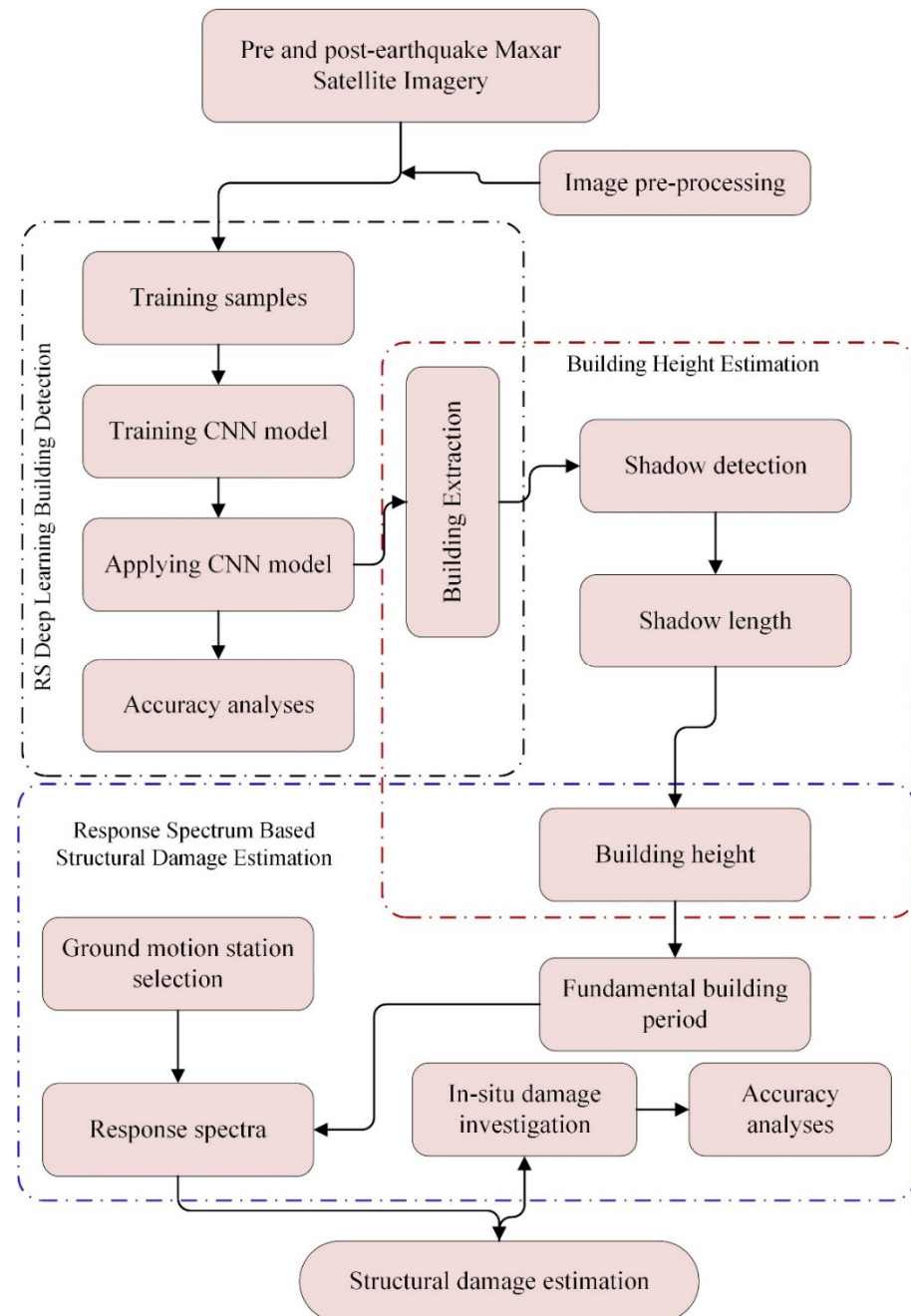


Figure 3. Flowchart of the methodology.

2.2.1. Remote Sensing Data and Techniques

Two satellite images, pre-earthquake (27 April 2020) and post-earthquake (3 November 2020), were provided by Maxar (DigitalGlobe company, Westminster, CO,

USA) with high-resolution (30 cm) and three bands (red, green, and blue, RGB) were used for the analyses.

The CNN workflow using Trimble's eCognition Developer 9.01 was applied to detect the buildings in the study area, based on the Google TensorFlow [30]. The analyses were done in a computer system with a 64-bit operating system, 16 GB RAM, and an Intel (R) Xeon (R) CPU E3-1535M v5 @ 3.60 GHz processor. The CNN model in eCognition was constructed of three different steps: (i) derivation of training samples, (ii) training the CNN model; (iii) applying the trained CNN model. For the training, 90×90 pixel samples were collected using the satellite imagery obtained from Maxar (Figure 4). A simple CNN model was created with one hidden layer with the highest correlation within the sample template.

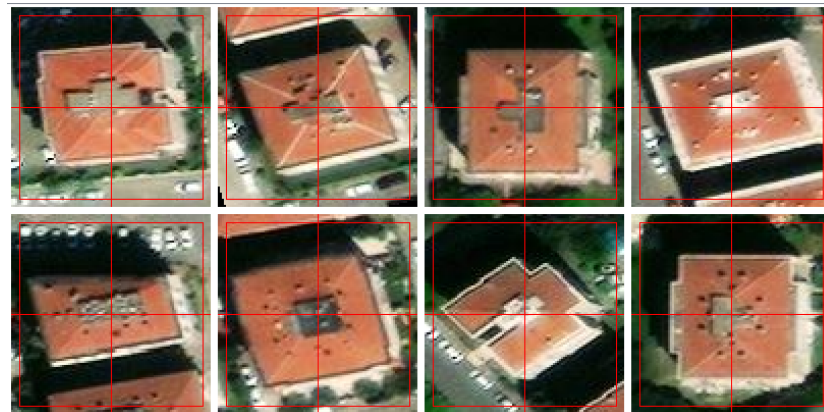


Figure 4. Example of 90×90 pixels samples generated from the CNN.

For the accuracy analyses, common evaluation statistics for binary classification were used. Namely, True Positives (TP) (a building is correctly identified), False Positives (FP) (a building is incorrectly identified; a commission error), and False Negatives (FN) (a building is missed; an omission error) parameters were taken into consideration. TP, FN, and FP indicate perfect identification, under-identification, and over-identification, respectively. Then the Precision (P), Recall (R), and F-score (F) were calculated. Precision (i.e., positive predictive value) describes the correctness of detected buildings and how well the algorithm dealt with FP (Equation (2)), Recall (i.e., sensitivity) describes the building detection rate and how well the algorithm dealt with FN (Equation (3)), and the F-score is the harmonic mean of Recall and Precision and reports the overall accuracy considering both commission and omission errors (Equation (4)) [30].

$$P = TP / (TP + FP) \quad (2)$$

$$R = TP / (TP + FN) \quad (3)$$

$$F\text{-score} = 2 \times ((P \times R) / (P + R)) \quad (4)$$

For the building heights, the length of the shadow of the buildings has been measured. Using the sun elevation angle of the first image ($62^\circ 34' 4.35''$) of the time of the passing of the satellite over the study area has been used for calculating the buildings' heights. The estimated heights of the buildings were calculated using Equation (5).

$$(\text{Height of the object}) = \tan(\text{Sun Elevation Angle}) \times (\text{Length of the shadow}) \quad (5)$$

2.2.2. Response Spectra-Based Damage Estimation

This study aims to propose a response spectra-based post-earthquake structural damage estimation approach. Thus, response spectra of stations located in the neighborhood of primarily affected urban areas (Bayrakli region; Adalet and Manavkuyu neighborhoods in Izmir) from the October 30 Samos earthquake were investigated. The strong ground motion was recorded by the extensive network of AFAD. In the Bayrakli region, there are

three seismic recording stations. Two of them are located on stiff soils (#3514 and #3520) having shear wave velocities of 836 and 875 m/s, respectively, and one (#3513) is on soft soil with 196 m/s. The study area is also on soft soil deposits similar to station #3513's location (Figure 5).

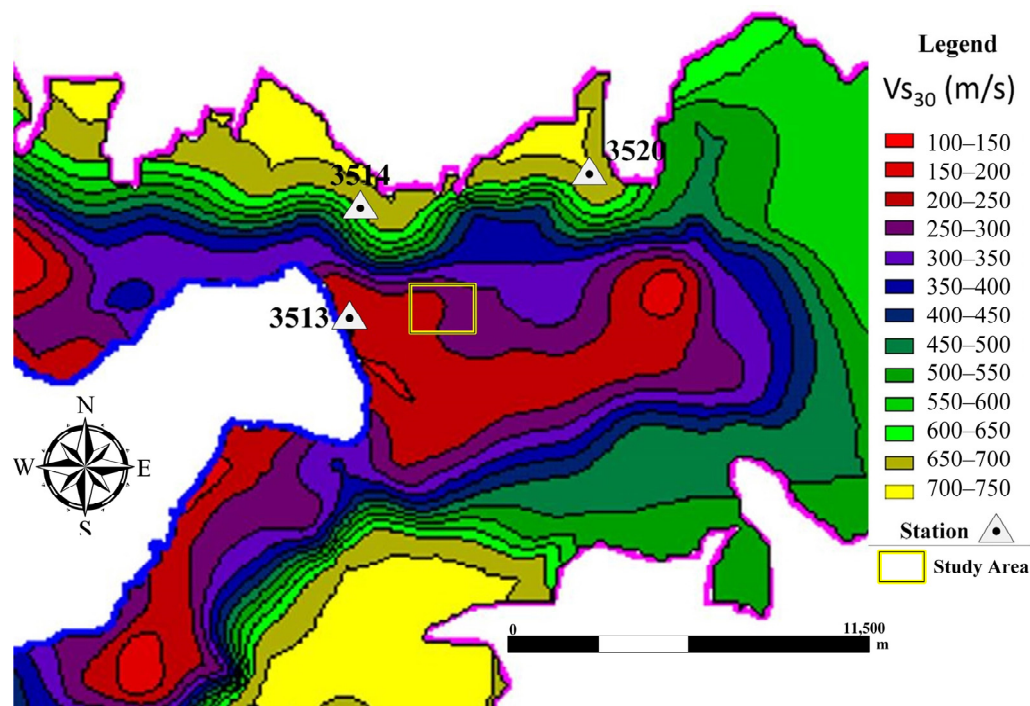


Figure 5. The distribution of V_{s30} (average shear wave velocity in the upper 30 m) map of the Inner Izmir Bay Basin modified from Izmir Earthquake Master Plan [31] and seismic recording stations around the study area in the Bayrakli region.

The elastic acceleration response spectra of stations #3513, #3514, and #3520 were plotted for their horizontal directions in Figure 6, strong ground motion records were provided from the Turkish Accelerometric Database and Analysis System (TADAS) [32]. Figure 6 also contains the elastic design spectra of the location of station #3513 according to Turkey Building Earthquake Code 2018 (TBEC-2018) [33] for soft and stiff soils. Additionally, the spectra for soft soils defined in the previous versions of the Turkish earthquake code (TEC-2007 [34], TEC-1997 [35], and TEC-1975 [36]) are shown in Figure 6, considering most of the collapsed buildings were constructed in the 1990s and were located on soft alluvial soils of the Bayrakli region. The design and response spectra were plotted with a damping ratio of 5%.

Comparing the design and response spectra, since the design spectra of the current and previous versions of Turkish code for both types of soil are well above the response spectra, and it can be noted that all versions of the code have well defined the seismic hazards of the region. Regardless of the hazard level for the collapsed buildings that were designed, they would not have collapsed if they had been designed following the seismic design principles of the current or previous versions of the governing building code. Moreover, there are buildings of similar typology nearby that did not collapse and were immediately reoccupied. It is very likely that the collapsed buildings, particularly those that experienced gravity (pancake) type failure, were not designed by the version of the code in force at the time of their construction and/or had structural and material-related deficiencies [27]. Figure 6 also shows that soft soil deposits in the Bayrakli region amplified the spectral accelerations. As a result of this amplification, the spectral accelerations on soft soils were approximately 2.5 times larger than those on the rock sites. Table 1 contains the information on recorded strong ground motions of the Samos earthquake for Bayrakli region stations.

In addition to spectral acceleration differences between the stations, Housner and Arias intensity and PGV values are significantly greater for #3513 (Table 1). The study area is also on soft soil deposits similar to station #3513's location (Figure 5). Therefore, station #3513 was selected as the critical station for applying the proposed rapid structural damage estimation approach in this study.

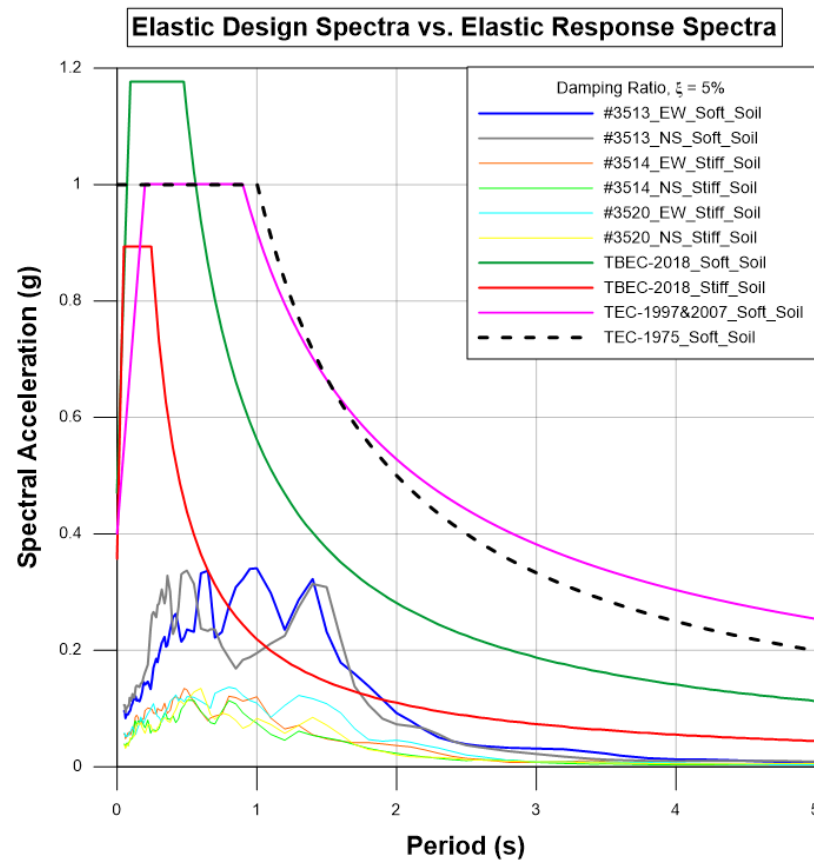


Figure 6. Comparison of the elastic acceleration response spectra of the recorded ground motion at the three stations of AFAD in the Bayrakli region against the design spectra of current and earlier versions of Turkish Seismic Codes at these locations.

Table 1. Information on recorded strong ground motions of the Samos earthquake for Bayrakli region stations [37].

Station Code	Rrup (km)	Repi (km)	Vs30 (m/s)	Comp.	PGA (cm/s ²)	PGV (cm/s)	PGD (cm)	Significant Duration (s)	Arias Intensity (cm/s)	Housner Intensity (cm)
3513	65.05	72.00	196	E-W	94.67	14.42	3.15	20.16	35.30	84.81
				N-S	106.28	17.11	2.90	20.59	33.17	79.76
				U-D	44.19	4.48	0.80	30.84	6.42	23.29
3514	66.62	73.39	836	E-W	56.02	6.41	1.31	23.75	4.58	28.26
				N-S	39.42	4.23	1.44	25.90	3.52	22.39
				U-D	25.15	1.94	0.73	27.17	2.10	10.91
3520	68.46	75.78	875	E-W	58.55	8.37	2.04	5.21	5.21	36.08
				N-S	36.11	4.65	1.13	3.60	3.60	24.21
				U-D	19.37	2.68	0.70	1.33	1.33	13.63

The response spectra of the ground motion recorded at station #3513 were thoroughly investigated. Figure 7 depicts response spectra of both horizontal components as well as their geometric mean. In addition, the fundamental vibration periods of various building types in and around the study area are demonstrated in Figure 7 to determine the critical period intervals in the response spectra. Especially the collapsed and heavily damaged mid-rise buildings were selected to investigate their fundamental periods and corresponding seismic demand based on the response spectra. During the earthquake, five mid-rise buildings in the study area and four nearby collapsed. The fundamental periods of those nine collapsed buildings range from 0.41 to 0.56 s. In the study area, there were four heavily damaged mid-rise buildings with fundamental periods ranging from 0.45 s to 0.49 s, and one mid-rise building with a period of 0.67 s did not sustain any damage. Low-rise buildings in the region have fundamental periods ranging from 0.09 s to 0.21 s, and a nearby high-rise building has a period of 1.07 s. Figure 8 shows their locations in the region. The fundamental vibration periods of the buildings were predicted based on their height using Equation (1). The building heights were calculated by implementing Equation (5) in the satellite images using remote sensing techniques.

Figure 7 shows three peak regions in the spectra where seismic demand is high: between 0.30 and 0.65 s, 0.85 and 1.15 s, and around 1.4 s. Notably, the elastic fundamental periods of collapsed and heavily damaged buildings are in the range of 0.40 and 0.65 s. Despite the presence of some substandard low-rise buildings, which have periods between 0.10 and 0.20 s in the study area, they were unaffected by the earthquake due to relatively low seismic demand. The other peaks of the spectra are around 1.00 and 1.40 s. There is only one building near the study area with a fundamental period of around 1.00 s (1.07 s), with a height of 55.12 m; it is the tallest building in the vicinity of the study area, and it suffered no damage as a result of the earthquake. Despite being severely shaken, no structural damage was discovered in the tall buildings in the Bayrakli region, about 30 buildings with heights between 100 m and 240 m [26] with periods approximately ranging between 2.00 to 4.50 s. Since there were no buildings with elastic fundamental periods between 1.00 and 1.40 s in the study area, the critical period interval in terms of seismic demand was set at 0.40 and 0.65 s. Buildings with fundamental periods between this range were labeled as “high-risk”. Assuming that those buildings are most likely to be damaged, they should be inspected primarily by the in situ damage assessment teams. Moreover, as seen in Figure 6, there is no such region as the peaks of response spectra of the ground motion is above the design spectra for the selected study area. Indeed, if there are any peaks above the design spectra, such regions would be chosen as the critical period intervals.

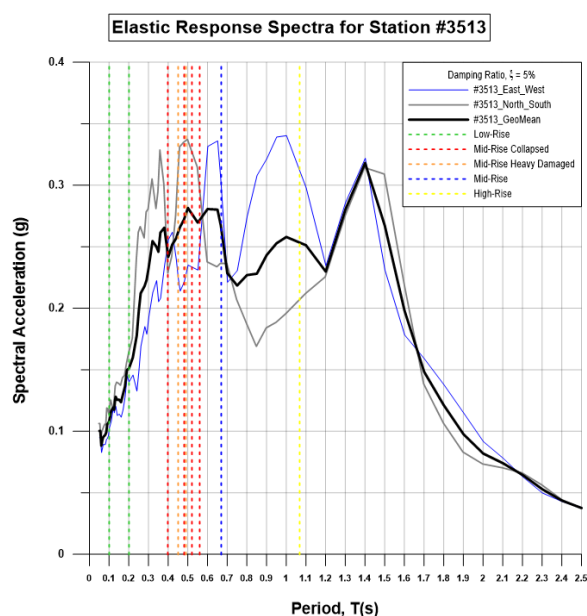


Figure 7. Response spectra of station #3513 and the fundamental periods of various building types in and around the study area.

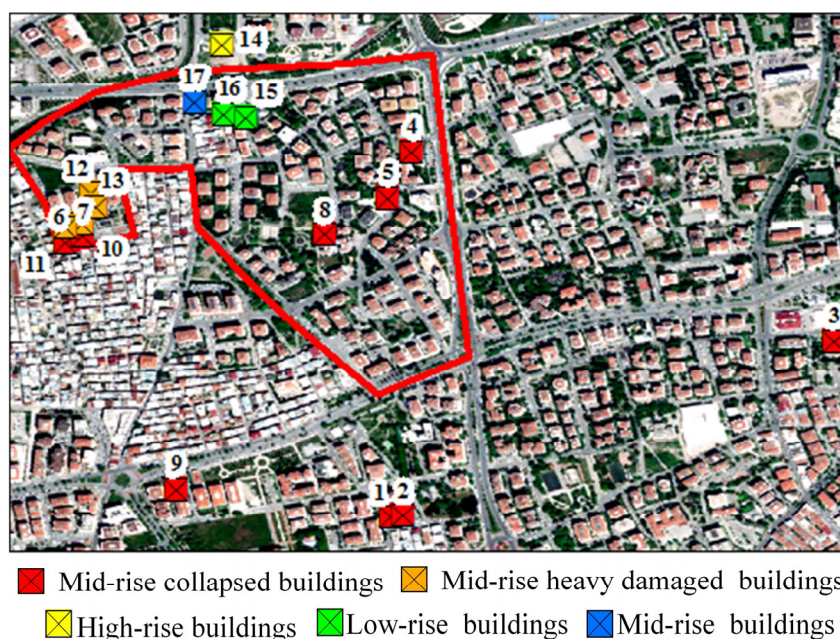


Figure 8. Locations of various building types (consistently color-coded with the fundamental periods of the buildings in Figure 7) in and around the study area.

3. Results

3.1. Remote Sensing

The building detection using CNN performed well with accuracy higher than 95% in both satellite images (Table 2). However, the results also showed some confusion between discrete and adjacent buildings. For example, some adjacent buildings were classified as one building in the first image, while in the second image, some of the adjacent buildings were classified as separate buildings. Since there is no visible boundary between adjacent buildings and usually have the same characteristics, the adjacent buildings classified as discrete buildings were considered correctly classified. Additionally, it should be mentioned that a group of low-rise adjacent buildings were not taken into consideration and are shown in the results as NA (Not Applicable).

Table 2. Accuracy assessment for the CNN building classification.

	Pre-Earthquake Image	Post-Earthquake Image
P	97.6	93.5
R	98.4	98.5
F-score	98.0	95.9

The classified images are shown in Figure 9. The CNN approach accurately detected most of the buildings in the study area. A total of 127 buildings were detected in the first image and 140 in the second image. This difference comes from the difference in the classification of the attached buildings. The number of TP (truly detected buildings) was 122 for the first image and 129 for the second image, FN (missed buildings) was two in both images. The visual inspection concluded that these buildings are significantly smaller than the other detected buildings. The three for the first, and nine for the second image buildings were FP (falsely classified buildings). In the first image, the falsely classified buildings were objects with similar characteristics as the buildings, such as red-colored basketball court. In contrast, in the second image, the falsely classified objects were generally tents set for the earthquake victims in open areas like parks and sports areas in the study area. Additionally, compared to the pre-earthquake image, the accuracy of the post-earthquake image has been negatively affected by the poor image quality, which resulted in slightly lower P values, and thus the overall F-score of the classification.

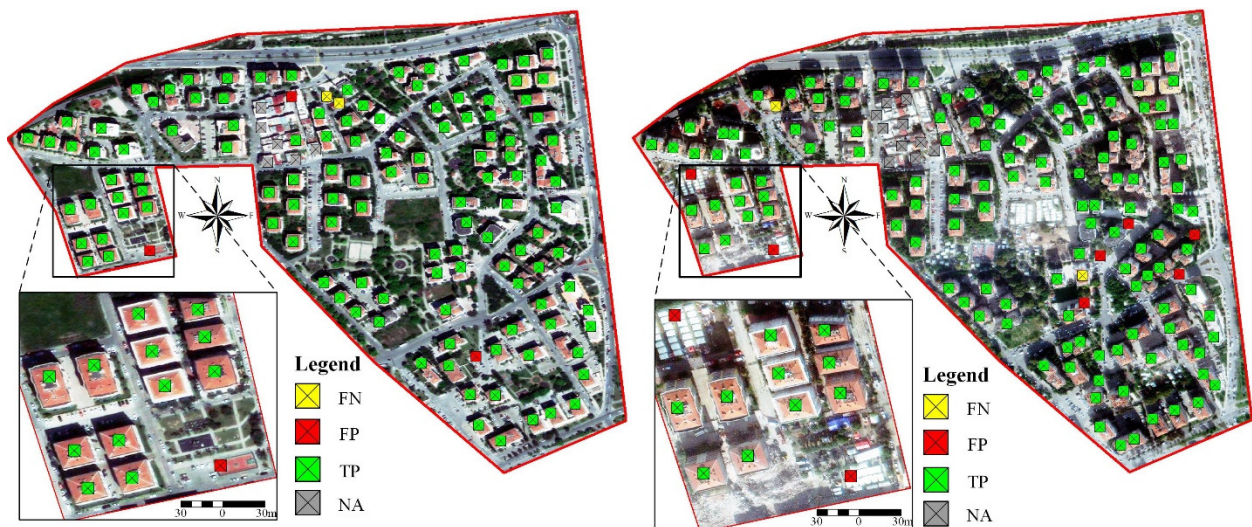


Figure 9. Pre (left) and post (right) earthquake building detection from Maxar satellite imagery.

3.2. Structural Damage Estimation Results

As stated in the “Response Spectra-Based Damage Estimation” section, buildings with fundamental periods between 0.40 and 0.65 s were labeled as “high risk” based on investigations conducted on the fundamental periods of collapsed and heavily damaged buildings and response spectra of the recorded ground motion at the critical station. As a result, those buildings are the most likely to be damaged and should be inspected first by in situ damage assessment teams. High-risk buildings are labeled with red color in Figure 10. Green and orange indicate low-risk buildings; green represents buildings with fundamental periods of less than 0.40 s, and orange represents buildings greater than 0.65 s. Estimation results were compared with the in situ damage assessment reports [38] prepared by the Republic of Turkey Ministry of Environment and Urbanization experts.

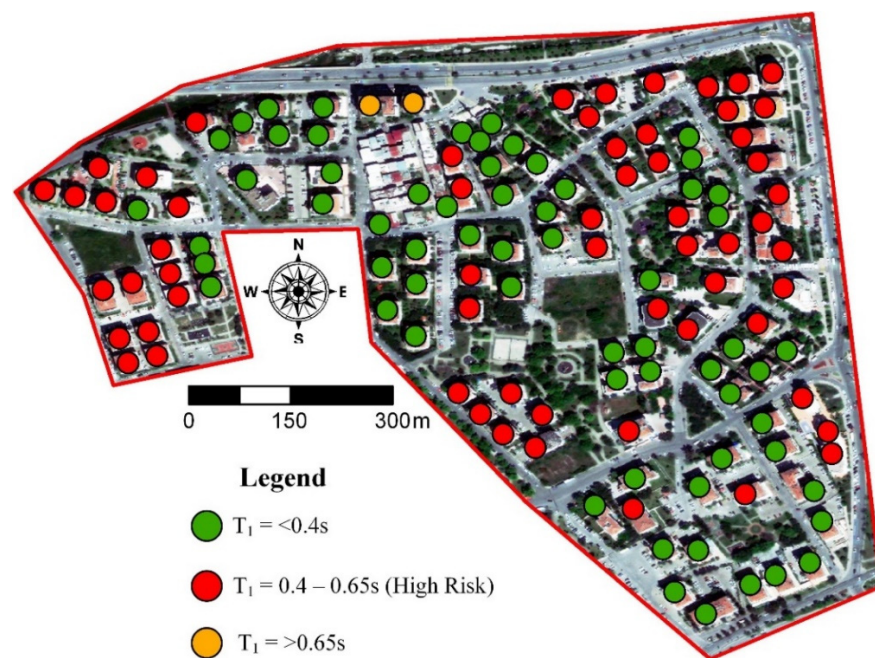


Figure 10. Structural damage estimation in the study area.

In order to evaluate the results, an accuracy assessment has been made using Equations (2)–(4). In the assessment, the predictions made in this research were compared with the on-site damage reports obtained from the Republic of Turkey Ministry of

Environment and Urbanization [38]. From 127 buildings, we were able to access damage reports of 117 buildings. In the comparison, collapsed, severely damaged, and moderately damaged buildings in the damage assessment reports were labeled as high-risk in this study. Buildings with minor damage and those with no damage were designated as low-risk buildings. TP represents the buildings that were correctly predicted to be high-risk and low-risk (69 buildings), FN represents the buildings that were incorrectly predicted to be low-risk (7 buildings). FP represents the buildings that were falsely predicted to be high-risk but were actually classified as low-risk based on the damage reports (39 buildings) (Figure 11). The accuracy assessment showed that the Recall of the method is 91%, the Precision is 64%, and the overall accuracy or the F-score is 75%.

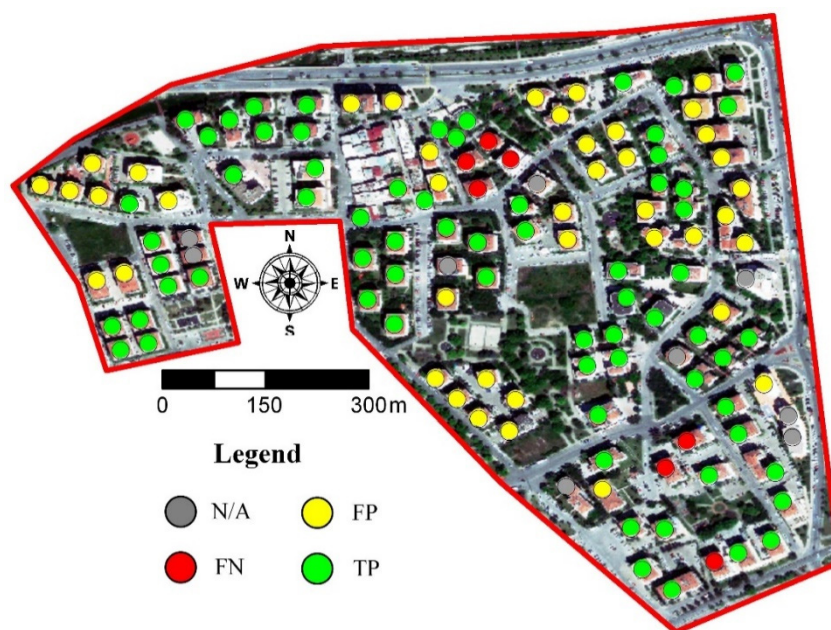


Figure 11. Accuracy assessment of structural damage estimation in the study area.

4. Discussion

The study aims to speed up the damage assessment process of critical buildings that can cause casualties in a possible strong aftershock; from this perspective, conventionally, the number of buildings that must have been investigated after the earthquake by in situ damage assessment experts were 127. If the proposed approach had been used, this number would have been reduced to 60. Because the proposed methodology suggests primarily investigating the potential high-risk buildings (Figure 10) due to their relatively high seismic demand, assuming that their seismic behavior is similar to those collapsed or severely damaged buildings in the region. Even if 39 of those 60 were classified as low-risk based on the in situ inspections, the necessary time spent by the damage assessment teams to detect the critical buildings would have been significantly reduced (more than 50%). It should be noted that in the proposed approach, the predicted seismic demand of the buildings is not compared with the capacity. Thus, the 39 buildings, classified as low-risk according to on-site inspections, can be considered as having higher seismic capacity than their collapsed and severely damaged counterparts. However, according to the on-site damage assessment reports, seven of the buildings classified as low-risk based on the proposed model were severely and/or moderately damaged; this number is meager in the total number of predictions. It corresponds to a 91% success rate in dealing with the false-negative predictions. In order to understand the reasons for the false-negative predictions, the photos of the seven buildings in the damage assessment reports were investigated in detail, and it was concluded that the decisions made by assessors for most of those seven buildings were questionable, even though, prior to this earthquake, the damage assessors were pre-trained for the first time in Turkey [37] by the Ministry of

Environment and Urbanization according to the methodologies developed by Ilki et al. [39] and Boduroglu et al. [40]. However, the damage assessment process is not an easy task due to many issues like varying experience and knowledge of the assessors. According to previous experiences in Turkey, in some cases, especially when the assessors have trouble deciding about the damage state of the building, they tend to choose heavy damage to avoid risks of a potential collapse of the building during strong aftershocks or future earthquakes. Sometimes the building owners also try to influence the assessors' decisions to be benefited from post-disaster help campaigns of the government. The reasons mentioned above may be argued to have influenced damage state decisions for some of the seven buildings. The methods developed by Ilki et al. [39] and Boduroglu et al. [40] aim to prevent such subjective decisions by providing a systematic, objective, and reliable seismic damage assessment system that results in the same structural damage level regardless of who makes the damage assessment.

In addition, it should be stated that, in the end, all of the buildings in the region must be inspected by in situ damage assessment teams. The proposed prioritization aims to provide an optimum allocation of time and resources after a catastrophic event for the civil protection units and decision-makers responsible for managing the consequences of the disaster. Instead of starting from the first building in the region, having a map produced by the proposed methodology would allow the decision-makers to divert the assessment teams primarily to the buildings expected to be severely damaged.

It is worth noting that some issues may be considered shortcomings of the approach, but they can be improved in future studies. For instance, in the proposed methodology, the classification of the expected damage is applied only based on the seismic demand, estimated from satellite-based remote sensing data and response spectra of the selected critical station in the region. The predicted seismic demand of the buildings is not compared with the capacity. When the rapid nature of the procedure and the idea of using remotely accessible data are taken into account, determining the seismic capacity of buildings is not consistent with the philosophy of the approach because it requires entering the buildings. The seismic capacity of the buildings or at least some indicators, like existing structural deficiencies and/or irregularities, can be provided from GIS-based building inventory databases if they exist for the investigated region. According to that information, a damage index can be defined. In some cases, the construction year can also be a good indicator if a milestone year can be designated for the region [41].

Another issue could be using the fundamental vibration period to estimate the seismic demand from response spectra which are designed to represent the SDOF system's response. It should be noted that most of the buildings in practice are MDOF systems, and different modes contribute to their behavior. However, it can be assumed that the fundamental vibration mode controls the seismic response, at least for the buildings whose response is not affected by the contribution of higher modes of vibration (mid-rise buildings) and the buildings without torsional irregularities. In addition, instead of using elastic values of fundamental periods, effective (yield) building periods can provide better damage predictions. However, it is not easy to identify the yield periods by empirical equations to the extent of usage in urban-level applications.

In the proposed methodology, the response spectra of nearby stations in the most affected area are used to estimate the seismic demand of the buildings, and it requires an extensive seismic recording network. For the regions with a limited strong ground motion network, some approaches such as empirical Ground Motion Prediction Models (GMPM) [42] or simulated datasets [25,43] could provide estimations on the hazard levels at locations where the actual motions are not recorded. In this way, the proposed approach can also be utilized for risk mitigation due to future events.

Without building inventory data or calculations, the collapsed and severely damaged reinforced concrete buildings' (7–10 floors) period range was considered between 0.60 and 1.50 s in some reports and papers published after the earthquake [2,37,44], assuming that the building damages correlated with the second and third peaks of station #3513's elastic

response spectra (Figure 7). However, in this study, the building heights were calculated by implementing Equation (5) over the satellite images using remote sensing techniques. Then, the elastic fundamental vibration periods of the buildings were predicted based on their heights using Equation (1). According to the predictions made in this study, the elastic fundamental periods of the collapsed and severely damaged buildings range between 0.40 and 0.65 s and this period interval correspond to the first peak of the response spectra of station #3513 that correlates similar demand with the second and third peaks (Figure 7). The practitioners in Turkey generally use the number of stories (N) above the ground to predict the elastic fundamental periods of RC buildings (T) using an empirical equation ($T = 0.1 N$) which was used in the 1975 version of the Turkish earthquake code TEC-1975 [36], NEHRP-94 and the National Building Code of Canada [45,46]. That correlates well with the equations derived from measurements conducted on moment-resisting RC frame buildings during the 1971 San Fernando earthquake, infilled with drywall, thus more flexible than Turkish counterparts. This equation overestimates the fundamental periods compared to Equation (1), which was developed by performing ambient vibration measurements on residential mid-rise reinforced concrete buildings with masonry infill walls in Eskisehir, Turkey. As being such, Equation (1) may represent the typical elastic dynamic characteristics of Turkish RC building stock.

Ordaz et al. [47] proposed an early earthquake damage assessment system for Mexico City. In their study, the number of stories gathered from the existing building inventory database of Mexico City has been used to predict the fundamental vibration period of the buildings, which makes the model dependent on a building inventory database. Similarly, the Izmir Metropolitan Municipality has a GIS building inventory database for the study area, and the building height information exists in the inventory. Nevertheless, the building heights were retrieved from the story numbers assuming the height of each story is the same, and it equals three meters. This assumption can lead to a significant difference from the actual building heights, especially for buildings with commercial units on the ground floors, which are very common in the study area, due to their relatively high story heights. Therefore, in this study, the calculated building heights from the satellite images were used instead of using existing building height information in the inventory. The proposed approach uses remote sensing techniques to estimate the building heights from satellite images that can be provided anywhere on the earth, so the proposed methodology can be applied regardless of having an inventory database that includes building height information for the region. The reliability of retrieving building heights from remote sensing data using shadows has been successfully proven in various studies with high accuracy [41,48].

The majority of existing earthquake rapid response systems estimate building damages after an earthquake using fragility curves. Developing fragility curves requires a well-established building database and a large number of nonlinear dynamic analyses performed on the categorized building classes [49]. A limited number of countries and cities have well-developed building inventories [3]. Being dependent on a building inventory and computationally very intensive can be considered a limitation for deriving fragility functions for a specific region. Another advantage of the proposed methodology is its flexibility to be applied with or without a building inventory database. The proposed approach can be used for the regions where the fragility curves do not exist.

5. Conclusions

A response spectra-based post-earthquake structural damage estimation method aided by satellite-based remote sensing data was proposed in this study. A case study application was implemented in the Bayrakli region, the most affected area in Izmir, Turkey, by the Samos earthquake on 30 October 2020. According to the findings of this study, the following conclusions and recommendations can be made:

- The proposed approach appears to be efficient in diverting the site inspectors to the buildings expected to be heavily damaged. The accuracy assessment showed that the

sensitivity (Recall) of the method is high (91%). The necessary time spent by the in situ damage assessment teams to detect the critical buildings that can cause casualties in a possible strong aftershock would have been significantly reduced (more than 50%) for the study area.

- The proposed approach uses remote sensing techniques to estimate the building heights from satellite images that can be provided anywhere on the earth, so the proposed methodology can be applied regardless of having an inventory database that includes building height information for the region.
- Integration with an existing building inventory in a GIS environment can provide more accurate results. Possible knowledge about the building capacity would be beneficial in addition to seismic demand provided from response spectra.
- The proposed approach can be used for the regions where the fragility curves do not exist.
- The critical seismic recording station selection is based on correlations between the selected region and the soil properties of the station locations and PGV, Housner, and Arias intensity values of the ground motions recorded at the surrounding stations. So, a dense seismic recording network is needed to conduct the proposed methodology, or empirical GMPM's or simulated datasets can be used.
- All peaks of the response spectra of ground motion at the selected critical station should be considered as crucial periods, especially if any of the peaks are above the design spectrum of the region.
- The empirical equation used to predict the elastic fundamental periods of the buildings should be region specific and represent the design spectra of the region and construction characteristics.
- Estimation of yield building periods can provide better damage predictions.
- The current state of the approach is limited to investigating RC buildings because of the used empirical period equation. Additionally, distinguishing masonry and RC buildings from each other using satellite images is a challenging task.
- The building height extraction methodology needs to be improved for the adjacent buildings and be automatized.

With the rapid development of remote sensing sensors and techniques, the results of the remote sensing classification can be improved in future studies as new data and new, more accurate classification techniques such as Mask RCNN [15], are becoming available every day. With the daily satellite imagery that can be easily obtained from various satellite sensors and updated drone images, post-earthquake data can be acquired in a short time, thus reducing the time required for in situ inspection. An automated method for height calculation from shadow information can be developed. Another option for this matter could be the use of ready-to-use data from urban digital twins if available. The proposed methodology would be of great importance in the case of automatization, and thus the results of the proposed methodology can be obtained within hours after the earthquake.

The results demonstrate that this approach can be used to speed up the damage assessment process, prioritizing the critical buildings based on their expected damage levels. The proposed prioritization aims to provide an optimum allocation of time and resources after a catastrophic event for the civil protection agencies and decision-makers responsible for managing the consequences of the disaster.

Author Contributions: The authors (O.K. and G.K.) contributed equally. All authors have read and agreed to the published version of the manuscript.

Funding: This study was supported by Eskisehir Technical University Scientific Research Projects Commission under grant No: 20ADP112, Project: "Building Inventory Information for Seismic Vulnerability Assessment Using Remote Sensing Techniques".

Informed Consent Statement: Not applicable.

Data Availability Statement: Not applicable.

Conflicts of Interest: The authors declare no conflict of interest.

References

1. Askan, A.; Gülerce, Z.; Roumelioti, Z.; Sotiriadis, D.; Melis, N.S.; Altindal, A.; Akbaş, B.; Sopaci, E.; Karimzadeh, S.; Kalogeras, I.; et al. The Samos Island (Aegean Sea) M7. 0 Earthquake: Analysis and engineering implications of strong motion data. *Bull. Earthq. Eng.* **2021**. [[CrossRef](#)]
2. Yakut, A.; Sucuoğlu, H.; Binici, B.; Canbay, E.; Donmez, C.; Ilki, A.; Caner, A.; Celik, O.C.; Ay, B. Performance of structures in İzmir after the Samos island earthquake. *Bull. Earthq. Eng.* **2021**. [[CrossRef](#)]
3. Erdik, M.; Şeşetyan, K.; Demircioğlu, M.; Hancılar, U.; Zülfişar, C. Rapid earthquake loss assessment after damaging earthquakes. *Soil Dyn. Earthq. Eng.* **2011**, *31*, 247–266. [[CrossRef](#)]
4. Tong, X.; Hong, Z.; Liu, S.; Zhang, X.; Xie, H.; Li, Z.; Yang, S.; Wang, W.; Bao, F. Building-damage detection using pre-and post-seismic high-resolution satellite stereo imagery: A case study of the May 2008 Wenchuan earthquake. *ISPRS J. Photogramm. Remote Sens.* **2012**, *68*, 13–27. [[CrossRef](#)]
5. Dong, L.; Shan, J. A comprehensive review of earthquake-induced building damage detection with remote sensing techniques. *ISPRS J. Photogramm. Remote Sens.* **2013**, *84*, 85–99. [[CrossRef](#)]
6. Karimzadeh, S.; Matsuoka, M. A Preliminary Damage Assessment Using Dual Path Synthetic Aperture Radar Analysis for the M 6.4 Petrinja Earthquake (2020), Croatia. *Remote Sens.* **2021**, *13*, 2267. [[CrossRef](#)]
7. Omarzadeh, D.; Karimzadeh, S.; Matsuoka, M.; Feizizadeh, B. Earthquake Aftermath from Very High-Resolution WorldView-2 Image and Semi-Automated Object-Based Image Analysis (Case Study: Kermanshah, Sarpol-e Zahab, Iran). *Remote Sens.* **2021**, *13*, 4272. [[CrossRef](#)]
8. Amini Amirkolae, H.; Arefi, H. CNN-based estimation of pre-and post-earthquake height models from single optical images for identification of collapsed buildings. *Remote Sens. Lett.* **2019**, *10*, 679–688. [[CrossRef](#)]
9. Tang, R.; Liu, H.; Wei, J.; Tang, W. Supervised learning with convolutional neural networks for hyperspectral visualization. *Remote Sens. Lett.* **2020**, *11*, 363–372. [[CrossRef](#)]
10. Li, W.; Fu, H.; Yu, L.; Cracknell, A. Deep learning based oil palm tree detection and counting for high-resolution remote sensing images. *Remote Sens.* **2017**, *9*, 22. [[CrossRef](#)]
11. Chen, B.; Xiao, X.; Li, X.; Pan, L.; Doughty, R.; Ma, J.; Dong, J.; Qin, Y.; Zhao, B.; Wu, Z.; et al. A mangrove forest map of China in 2015: Analysis of time series Landsat 7/8 and Sentinel-1A imagery in Google Earth Engine cloud computing platform. *ISPRS J. Photogramm. Remote Sens.* **2017**, *131*, 104–120. [[CrossRef](#)]
12. Wang, Z.; Underwood, J.; Walsh, K.B. Machine vision assessment of mango orchard flowering. *Comput. Electron. Agric.* **2018**, *151*, 501–511. [[CrossRef](#)]
13. Mubin, N.A.; Nadarajoo, E.; Shafri, H.Z.M.; Hamedianfar, A. Young and mature oil palm tree detection and counting using convolutional neural network deep learning method. *Int. J. Remote Sens.* **2019**, *40*, 7500–7515. [[CrossRef](#)]
14. Timilsina, S.; Sharma, S.; Aryal, J. Mapping urban trees within cadastral parcels using an object-based convolutional neural network. *ISPRS Ann. Photogramm. Remote Sens. Spat. Inf. Sci.* **2019**, *4*, 111–117. [[CrossRef](#)]
15. Ocer, N.E.; Kaplan, G.; Erdem, F.; Kucuk Matci, D.; Avdan, U. Tree extraction from multi-scale UAV images using Mask R-CNN with FPN. *Remote Sens. Lett.* **2020**, *11*, 847–856. [[CrossRef](#)]
16. Zhang, Q.; Wang, Y.; Liu, Q.; Liu, X.; Wang, W. CNN based suburban building detection using monocular high resolution Google Earth images. In Proceedings of the 2016 IEEE International Geoscience and Remote Sensing Symposium (IGARSS), Beijing, China, 10–15 July 2016.
17. Hu, Y.; Guo, F. Building Extraction Using Mask Scoring R-CNN Network. In Proceedings of the 3rd International Conference on Computer Science and Application Engineering, Sanya, China, 22–24 October 2019.
18. Nie, S.; Jiang, Z.; Zhang, H.; Cai, B.; Yao, Y. Inshore ship detection based on mask R-CNN. In Proceedings of the IGARSS 2018–2018 IEEE International Geoscience and Remote Sensing Symposium, Valencia, Spain, 22–27 July 2018.
19. Nie, X.; Duan, M.; Ding, H.; Hu, B.; Wong, E.K. Attention Mask R-CNN for Ship Detection and Segmentation From Remote Sensing Images. *IEEE Access* **2020**, *8*, 9325–9334. [[CrossRef](#)]
20. Chopra, A.K. Elastic response spectrum: A historical note. *Earthq. Eng. Struct. Dyn.* **2007**, *36*, 3–12. [[CrossRef](#)]
21. Bommer, J.J.; Boore, D.M. *Engineering Geology/Seismology, Encyclopedia of Geology*; Elsevier Academic: Oxford, UK, 2005; pp. 499–514.
22. Pan, T.-C.; Goh, K.S.; Megawati, K. Empirical relationships between natural vibration period and height of buildings in Singapore. *Earthq. Eng. Struct. Dyn.* **2014**, *43*, 449–465. [[CrossRef](#)]
23. Hong, L.-L.; Hwang, W.-L. Empirical formula for fundamental vibration periods of reinforced concrete buildings in Taiwan. *Earthq. Eng. Struct. Dyn.* **2000**, *29*, 327–337. [[CrossRef](#)]
24. Kaplan, O.; Guney, Y.; Dogangun, A. A period-height relationship for newly constructed mid-rise reinforced concrete buildings in Turkey. *Eng. Struct.* **2021**, *232*, 111807. [[CrossRef](#)]
25. Akinci, A.; Cheloni, D.; Dindar, A. The 30 October 2020, M7. 0 Samos Island (Eastern Aegean Sea) Earthquake: Effects of source rupture, path and local-site conditions on the observed and simulated ground motions. *Bull. Earthq. Eng.* **2021**, *19*, 4745–4771. [[CrossRef](#)]
26. Erdik, M.; Demircioğlu, M.; Cüneyt, T. Forensic Analysis Reveals the Causes of Building Damage in İzmir in the Oct. 30 Aegean Sea Earthquake. 2020. Temblor Website. Available online: <https://temblor.net/earthquake-insights/forensic-analysis-reveals-the-causes-of-building-damage-in-izmir-in-the-oct-30-aegean-sea-earthquake-12098/> (accessed on 25 October 2021).

27. Günay, S.; Mosalam, K.M.; Archbold, J.; Dilsiz, A.; Beyazit, A.Y.; Wilfrid, G.D.; Gupta, A.; Concern, O.; Hassan, W.; María, S.; et al. StEER Preliminary Virtual Reconnaissance Report (PVRR): Aegean Sea Earthquake (M7.0), 30 October 2020. Available online: <https://www.designsafe-ci.org/data/browser/public/designsafe.storage.published/PRJ-2953/#details-4779265402462334485-242ac116-0001-012> (accessed on 25 October 2021).
28. Virghileanu, M.; Săvulescu, I.; Mihai, B.-A.; Nistor, C.; Dobre, R. Nitrogen dioxide (NO₂) pollution monitoring with sentinel-5p satellite imagery over europe during the coronavirus pandemic outbreak. *Remote Sens.* **2020**, *12*, 3575. [CrossRef]
29. CNN. Powerful Earthquake Jolts Turkey and Greece, Killing at Least 27. 31 October 2020. Available online: <https://edition.cnn.com/2020/10/30/europe/earthquake-greece-turkey-aegean-intl/index.html> (accessed on 25 October 2021).
30. Csillik, O.; Cherbini, J.; Johnson, R.; Lyons, A.; Kelly, M. Identification of citrus trees from unmanned aerial vehicle imagery using convolutional neural networks. *Drones* **2018**, *2*, 39. [CrossRef]
31. Metropolitan Municipality of Izmir (MMI) Izmir Earthquake Masterplan. 2000. Available online: <http://www.izmir.bel.tr/izmirdeprem/izmirrapor.htm> (accessed on 25 October 2021). (In Turkish)
32. Turkish Accelerometric Database and Analysis System (TADAS). TADAS 2021. Available online: <https://tadas.afad.gov.tr/login> (accessed on 1 November 2021).
33. TBEC-2018. *Turkey Building Earthquake Code*; AFAD, Ministry of Interior, Disaster and Emergency Management Presidency: Ankara, Turkey, 2018.
34. *Turkish Earthquake Code (TEC-2007): Specifications for Buildings to Be Built in Seismic Areas*; Ministry of Public Works and Settlement: Ankara, Turkey, 2007. (In Turkish)
35. *Turkish Earthquake Resistant Design Code (TEC-1997): Specifications for Structures to Be Built in Disaster Areas*; Ministry of Public Works and Settlement: Ankara, Turkey, 1997. (In Turkish)
36. *Turkish Earthquake Code (TEC-1975): Specifications for Buildings to Be Built in Seismic Areas*; Ministry of Public Works and Settlement: Ankara, Turkey, 1975. (In Turkish)
37. Onder Cetin, K.; Mylonakis, G.; Sextos, A.; Stewart, J.P. Seismological and Engineering Effects of the M 7.0 Samos Island (Aegean Sea) Earthquake. Available online: http://learningfromearthquakes.org/images/earthquakes/2020_Samos_Greece_Izmir_Turkey/Samos_Island_Earthquake_Final_Report.pdf (accessed on 25 October 2021).
38. Stratoulis, D.; Nuthammachot, N. Air quality development during the COVID-19 pandemic over a medium-sized urban area in Thailand. *Sci. Total Environ.* **2020**, *746*, 141320. [CrossRef]
39. Ilki, A.; Halici, O.; Kupcu, E.; Comert, M.; Demir, C. Modifications on seismic damage assessment system of TCIP based on reparability. In Proceedings of the 17th World Conference on Earthquake Engineering 17WCEE, Sendai, Japan, 22 April 2020.
40. Boduroglu, H.; Ozdemir, P.; Binbir, E.; Ilki, A. Seismic damage assessment methodology developed for Turkish compulsory insurance system. In Proceedings of the 9th Annual International Conference of the International Institute for Infrastructure Renewal and Reconstruction, Brisbane, Australia, 8–10 July 2013.
41. Kaplan, G.; Kaplan, O. PlanetScope Imagery for Extracting Building Inventory Information. *Environ. Sci. Proc.* **2021**, *5*, 19. [CrossRef]
42. Boore, D.M.; Stewart, J.P.; Skarlatoudis, A.A.; Seyhan, E.; Margaris, B.; Theodoulidis, N.; Scordilis, E.; Kalogeras, I.; Klimis, N.; Melis, N.S. A ground-motion prediction model for shallow crustal earthquakes in Greece. *Bull. Seismol. Soc. Am.* **2021**, *111*, 857–874. [CrossRef]
43. Karimzadeh, S.; Askan, A.; Erberik, M.A.; Yakut, A. Seismic damage assessment based on regional synthetic ground motion dataset: A case study for Erzincan, Turkey. *Nat. Hazards* **2018**, *92*, 1371–1397. [CrossRef]
44. Bayhan, B.; Avci, E.; Kayı, D.B. EGE DENİZİ SEFERİHİSAR AÇIKLIKLARI M6.6 DEPREMİ 30 EKİM 2020 YAPI ÖN DEĞERLENDİRME RAPORU; Bursa Teknik Üniversitesi, Deprem Mühendisliği Uygulama ve Araştırma Merkezi, Bursa, Turkey, 2020. (In Turkish). Available online: https://depo.btu.edu.tr/dosyalar/btu/Dosyalar/Rapor_Bursa.Teknik.Uni.Deprem.2020.10.30.pdf (accessed on 25 October 2021).
45. *National Earthquake Hazards Reduction Program: Recommended Provisions for the Development of Seismic Regulations for New Buildings*; Building Seismic Safety Council: Washington, DC, USA, 1994.
46. *National Research Council: The National Building Code (NBC)*; National Research Council: Ottawa, ON, Canada, 1995.
47. Ordaz, M.; Reinoso, E.; Jaimes, M.A.; Alcántara, L.; Pérez, C. High-resolution early earthquake damage assessment system for Mexico City based on a single-station. *Geofísica Int.* **2017**, *56*, 117–135. [CrossRef]
48. Comert, R.; Kaplan, O. Object Based Building Extraction And Building Period Estimation from Unmanned Aerial Vehicle Data. In Proceedings of the ISPRS Annals of the Photogrammetry, Remote Sensing and Spatial Information Sciences, Beijing, China, 7–10 May 2018.
49. Rossetto, T.; Elnashai, A. A new analytical procedure for the derivation of displacement-based vulnerability curves for populations of RC structures. *Eng. Struct.* **2005**, *27*, 397–409. [CrossRef]